Synthesis of high-density polyethylene/rGO-CNT-Fe nanocomposites with outstanding magnetic and electrical properties

Article *in* Journal of Applied Polymer Science · June 2017

DOI: 10.1002/app.45382

CITATIONS
4

READS
58

1 author:

Muhammad Nisar
Pontificia Universidade Católica do Rio Grande do Sul
8 PUBLICATIONS **44** CITATIONS

SEE PROFILE

Journal of Applied Polymer Science

Synthesis of high-density polyethylene/rGO-CNT-Fe nanocomposites with outstanding magnetic and electrical properties

Muhammad Nisar,[1] Carlos Pérez Bergmann,[2] Julian Geshev,[3] Raúl Quijada,[4] Thuany Maraschin,[5] Nara R. de Souza Basso,[5] Eliana G. Barrera,[1] Griselda Barrera Galland[1]

[1]Instituto de Química, Universidade Federal do Rio Grande do Sul, Porto Alegre 91501-970, Brazil
[2]Laboratório de Materiais Cerâmicos, Departamento de Materiais, Universidade Federal do Rio Grande do Sul, Porto Alegre, Brazil
[3]Instituto de Física, Universidade Federal do Rio Grande do Sul, Porto Alegre 91501-970, Brazil
[4]Departamento de Ingeniería Química y Biotecnología, Facultad de Ciencias Físicas y Matemáticas, Universidad de Chile, Santiago, Chile
[5]Faculdade de Química, Pontifícia Universidade Católica do Rio Grande do Sul, Porto Alegre 90619-900, Brazil
Correspondence to: G. B. Galland (E-mail: griselda.barrera@ufrgs.br)

ABSTRACT: Semi-conducting polyethylene (PE) nanocomposites with outstanding magnetic properties at room temperature were synthesized. These exceptional properties, for a diamagnetic and insulating matrix as PE, were obtained by polymerizing ethylene in the presence of a catalytic system formed by a metallocene catalyst supported on a mixture of reduced graphene oxide (rGO) and carbon nanotubes with encapsulated iron (CNT-Fe). It was used a constant and very low amount of CNT-Fe, obtained by vapor chemical deposition using ferrocene. The percolation threshold, to achieve conductivity, was obtained using a variable amount of rGO. The nanocomposites were semiconductors with the addition of 2.8 wt % and 6.0 wt % of the filler, with electrical conductivities of 4.99 $\times$ 10^{-6} S cm^{-1} and 7.29 $\times$ 10^{-4} S cm^{-1}, respectively. Very high coercivity values of 890–980 Oe at room temperature were achieved by the presence of only 0.04–0.06 wt % of iron in the nanocomposites. The novelty of this work is the production of a thermoplastic with both, magnetic and electric properties at room temperature, by the use of two fillers, that is rGO and CNT-Fe. The use of a small amount of CNT-Fe to produce the magnetic properties and variable amount of rGO to introduce the electrical conductivity in PE matrix let to balance both properties. The encapsulation strategy used to obtain Fe in CNT, protect Fe from easy oxidation and aggregation. © 2017 Wiley Periodicals, Inc. J. Appl. Polym. Sci. **2017**, *134*, 45382.

KEYWORDS: fullerenes; graphene; magnetism and magnetic properties; nanotubes; polyolefins; thermogravimetric analysis (TGA)

Received 27 January 2017; accepted 5 May 2017
DOI: 10.1002/app.45382

INTRODUCTION

Polymer nanocomposites are hybrid materials formed by the dispersion of inorganic fillers, in the nanometric scale, in polymeric matrixes.[1] The combination of organic polymer and inorganic fillers can improve the properties of the nanocomposite such as magnetic, thermal, dielectric, mechanical, or optical depending on the filler used.[2] Among the polymeric matrixes, polyethylene (PE) has attracted considerable attention because of its low cost, recyclability, easy processing, and versatility. The addition of fillers can broaden the application range of PE by improving its properties such as its gas barrier and thermal stability or by adding new properties such as electrical conductivity.[3] Likewise, extensive research work has been carried out using carbon nanotubes (CNTs) as reinforcements in polymers because of their outstanding tensile properties.[4] The CNTs closed in a tubular shaped having a single graphite sheet are termed as single-walled carbon nanotubes (SWCNTs), where as those consisting of multiple graphite sheets are called multiwalled carbon nanotubes (MWCNTs).[5] Nevertheless, the expected transmission of the properties from the filler to the polymer matrix is still an issue of discussion owing to several drawbacks, such as the difficult dispersion of CNTs in viscous solutions, the high production cost,[6] and the caged structure of the CNTs.[7] Although functionalization of CNTs is considered to be a possible solution, it leads to the destruction of the caged structure of the CNTs, which in turn reduces the tensile strength.[8] The CNTs/polymer nanocomposites with PE, polymethylmethcrylate, polyamide, and polyurethane have been prepared using different methods such as melt mixing, electro spinning, graft, and *in situ* polymerization to enhance various properties.[9]

The discovery of graphene has opened a new area of research in polymer nanocomposites owing to its tremendous physical properties.[10] Graphene has triggered enormous interest in many technological fields such as electronics, energy storage and conversion, sensors, capacitors, and composites materials.[11,12]

Therefore, graphene is a nanofiller with the potential to improve the properties of neat polymers,[13] but obtaining adequate-quality graphene or few graphene nanosheets at a reasonable cost is a major issue to deal with. Some current production routes include chemical vapor deposition, CO reduction, and the exfoliation of graphite. The latter method is the only one that can provide large quantities of graphene at low cost and is the one used to obtain nanocomposites.[14] Hassan *et al.*[15] reported the production of high-yield graphene nanosheets from expanded graphite using aqueous phase exfoliation method. Han *et al.*[16] modified thermally reduced graphene with stearic acid to enhance its lipophilicity. Similarly, some researchers investigated the compatibility of thermally reduced graphene with multiblock copolyesters and graphene/polyaniline.[17,18] The addition of graphite oxide (GO) as an effective fire retardant of epoxy resin has been also reported, by controlling the degree of oxidation the chemical structure of GO can be varied.[19]

Furthermore, magnetic polymer nanocomposites have also attracted the interest of both academic and industrial researchers. Magnetic polymer nanocomposites can be obtained by the incorporation of magnetic elements such as nickel, cobalt, and iron into a non-magnetic polymer matrix by using different polymerization methods, including *in situ* polymerization, surface-initiated polymerization, solution blending, ball milling, surface wetting methods, and ion exchange techniques.[20] Although iron-based magnetic nanoparticles (NPs) are most-abundantly used, there are problems in their use owing to easy oxidation and aggregation. Encapsulation of iron NPs into a non-magnetic carbon shell is an alternative to address this issue.[2] Recently, Osorio and Bergmann[21] and Osorio *et al.*[22] optimized the synthesis of CNTs with ferrocene, using silica nanopowders with different surface areas as a substrate, obtaining CNTs with iron encapsulated (CNT-Fe). In a recent work, we used those CNT-Fe to obtain PE nanocomposites with magnetic properties. It was shown that 0.9 wt % of CNT-Fe in PE was enough to obtain rather high coercivity values (~1000 Oe), but it was insufficient to generate electrical conductivity.[23]

Our research group is extensively involved in graphene-based polyolefin nanocomposites using *in situ* polymerization with metallocene catalysts.[24–27] In the present work, we focus on a dual stimuli-responsive material under electric and magnetic fields using reduced graphene oxide (rGO) and iron encapsulated carbon nanotubes (CNT-Fe) as fillers. A metallocene catalyst was immobilized on a mixture of variable amounts of rGO and a small amount of CNT-Fe to polymerize ethylene aiming to simultaneously obtain a thermoplastic with conductive and magnetic properties. This multifunctional material has potential to be applied as sensors in medicine and in electronic devices, low-temperature heaters, energy storage devices,[28] solar cells, magnetic recording materials,[29] magnetic sensors,[30] and microwave absorbers,[31] in the aerospace and automotive industries.

EXPERIMENTAL

Materials

All materials were handled under deoxygenated dry argon using standard schlenk tube techniques. Flakes of graphite (Grafine 99200, FN) (average diameter $\leq$150 microns) were provided by Nacional de Grafite Ltd. (Brazil). Sulfuric acid, nitric acid, hydrochloric acid, and potassium chlorate were purchased from Merck, Sao Paulo, Brazil. Metallic sodium and benzophenone were used for the distillation of toluene. Methylaluminoxane (MAO) (Sigma Aldrich, Brazil, 4.6 wt % Al solution in toluene) and bis(*n*-butyl)cyclopentadienylzirconium dichloride ($(n\text{-BuCp})_2ZrCl_2$) (Sigma Aldrich, Brazil) were used as received.

Graphene Oxide Synthesis and Thermal Reduction

Graphene oxide was synthesized from flakes (FK) using a modified Staudenmaier method,[32,33] where the time of oxidation was changed from 96 to 24 h. To obtain rGO, the GO was heated at 600 °C for 3 s in an oven, using a closed quartz ampoule under normal atmosphere. Complete characterization of rGO can be found in the work by Pavoski *et al.*,[33] but for sake of clarity, we added X-ray diffraction (XRD) and Raman of this material in the Supporting Information Figures S1 and S2, respectively. In accordance with the previous work,[33] this rGO has 27% of oxygen calculated by elementary analysis.

Carbon Nanotube Synthesis

The CNTs containing iron (CNT-Fe) were synthesized by Chemical Vapor Deposition (CVD), where ferrocene was used as a precursor and silica as a support. The reaction time was approximately 2 min and the temperature was increased up to 750 °C. The detailed method of synthesis of these CNTs and complete characterization were published in the work by Osorio and Bergmann[21] and Osorio *et al.*[22]

Support of the Catalyst

Variable amount of rGO, between 71 and 333 mg, and around 25 mg of CNT-Fe were placed in a schlenk vessel with toluene using argon atmosphere and sonicated with an ultrasound bath (Ultracleaner 1600A, Unique, Brazil) operating at 40 kHz for 8 h at room temperature. The rGO-CNT-Fe was sonicated for 30 min more with the addition of 15 wt % MAO. In the next step, $(n\text{-BuCp})_2ZrCl_2$ was added in an amount of 2 wt % Zr/rGO-CNT-Fe, followed by 2 h of stirring at 60 °C. The solid was then decanted and the supernatant eliminated, and washed twice with toluene. Subsequently, $(n\text{-BuCp})_2ZrCl_2$/rGO-CNT-Fe was used as the catalyst system for the polymerization of ethylene.

Polymerization Reaction

Polymerization was carried out in a 300 mL reactor (Parr Instrument Company, IL). Toluene was used as the solvent, and an extra amount of MAO (Al/Zr = 100) was added as the scavenger. The reactions were carried out at 25 °C, using ethylene pressure of 3 bar for 30 min. The rGO-CNT-Fe previously treated with $(n\text{-BuCp})_2ZrCl_2$ was added as the filler and catalyst of the reaction.

CHARACTERIZATION

Transmission electronic microscopy (TEM) analysis was performed using a transmission electron microscope (JEOL 1200 ExII) operated at 120 kV. Samples were prepared by deposition of a solution drop on a grid (CNTs and rGO) or from ultrathin films (~50 nm) cut under cryogenic conditions with a Leica Ultracut UCT microtome at −70 °C and placed on a grid (polymeric nanocomposites). Scanning electron microscopy (SEM) was performed using a Phillips XL30 microscope operating at 20 kV. Samples were prepared by deposition on an aluminum stub and gold metallization.

The amount of zirconium deposited on the surface of the filler was investigated by inductive coupled plasma emission spectroscopy (ICP) in a Perkin–Elmer, Optima 7320.

Differential scanning calorimetric (DSC) analysis was performed using a Perkin–Elmer differential calorimeter (model DSC Q20) operating at a heating rate of 20 °C/min and a temperature range of 0–180 °C. The crystallization temperature, T_c, and the melting temperature, T_m, were determined in the second and third scans, respectively, and the degree of crystallinity was calculated from the enthalpy of fusion data obtained from the DSC curves (293 J/g was used for 100% crystalline material).

The thermal stability of the samples was investigated using SDT Q600 thermal analyzer Q20 (TA Instruments, USA). This analysis was performed under nitrogen (50 mL/min) at a scanning rate of 20 °C/min from 0 to 800 °C.

The molecular weights were obtained with a Waters Alliance GPC 2000 instrument equipped with three Styragel HT-type columns (HT3, HT5, and HT6E). 1,2,4-Trichlorobenzene was used as the solvent with a flow rate of 1 mL/min at a temperature of 135 °C. The columns were calibrated with polystyrene standards.

The determination of Fe on the CNTs and polymers was carried out by High Resolution-Continuum Source Graphite Fournace Atomic Absorption Spectroscopy (HR-CS GF AAS) by direct solid sampling (SS) using a contrAA 700 high-resolution continuum source atomic absorption spectrometer (Analytik Jena AG, Jena, Germany). The samples were directly weighed, without any prior preparation step, on pyrolytically coated graphite tubes. A preadjusted pair of tweezers, which is part of the SSA 6 manual solid sampling accessory (Analytik Jena), was used to transfer the platforms to the atomizer. The program temperatures and method used were followed and adapted from the literature.[34] A 10 µL volume of a mixture of 20 µg Pd + 12 µg Mg was used as the chemical modifier dosed onto the sample prior to platform introduction into the atomizer. Pyrolysis and atomization temperatures were 800 and 2500 °C, respectively, using the 283.245 nm line and only the central pixel for evaluation.

For the electric resistivity, a megohmmeter (Megger BM11) with a highest voltage of 1200 V was used. With this set-up, the standard two-point method was used. For each electrical value displayed in this contribution, at least four samples were prepared and four measurements for each one were carried out. In general, differences around one order of magnitude were detected in the non-percolated samples having low conductivity values ($\sim 10^{-9}$ S/cm). For percolated samples, the experimental error for conductivities was less than 50%. For these tests, samples of size 40 mm × 16 mm and thickness 1 mm were used.

The magnetic characterization of the nanocomposites was performed using an EZ9 MicroSense vibrating sample magnetometer (VSM) at room temperature with a magnetic field (H) ranging from −20 kOe to +20 kOe.

RESULTS AND DISCUSSION

PE nanocomposites, with variable amounts of rGO and fixed amount of CNT-Fe, were prepared by *in situ* polymerization using $(n\text{-BuCp})_2ZrCl_2$ as the catalyst supported in the filler (rGO and CNT-Fe) impregnated by MAO. The combination of the both rGO and CNT-Fe were used to prepare a dual stimuli-responsive material under electric and magnetic fields. The synthetic route of the magnetic material (CNT-Fe) is apparently harder and time consuming as compared with the preparation of rGO by the exfoliation technique. In fact, rGO comes from graphite, which is a cheap source, and does not require complicated steps for its synthesis. On the other hand, the synthesis of CNT-Fe requires more expensive reagents and is time consuming because each synthesis gives only few amounts of material. A small amount of CNT-Fe (<1%) is enough to produce good magnetic properties but it is not enough to attain percolation to have electrical conductivity.[23] Consequently, the idea of using the combination of these two carbon materials aims to use the rGO to generate a conductive network in the PE matrix and a small amount of CNT-Fe to convert the diamagnetic PE matrix to a ferromagnetic one. The small amount of CNT-Fe used was previously mixed with rGO, thus the support is constituted mainly of rGO. The interaction between CNT-Fe and rGO may consists π-interactions between graphenes. The main filler, rGO, has also the function to support the catalyst. The method used was the same published by Mülhaupt and coworkers[35] and consist in bonding and coating the surface of rGO with the cocatalyst, MAO. The ionic interaction between the catalyst and MAO[36] produces the catalytic site from which the PE grows. The characterization of rGO used was published in a previous work[33] and consist of 27% of oxygen, mainly hydroxyl groups that are essential to bond the MAO. PE/rGO-CNT-Fe nanocomposites with filler contents, calculated from the polymer yield, were in the range of 1.3–6.0 wt % (Table I) (Digital images, XRD and Raman of the materials can be seen in Supporting Information Figures S3–S5). The catalytic activities, obtained after taking into account the supported amount of Zr obtained by ICP, showed that there is a deactivation of the catalytic system with the increase in the filler content. This behavior has already been seen in polymerizations with rGO owing to the presence of some oxygen functional groups that remain in the rGO and deactivate part of the catalyst even with the protection of MAO.[14] Even though there is some deactivation of the catalyst all the catalytic activities can be considered very high.

Table I also shows the thermal properties of the PE and its nanocomposites. The melting temperatures of the nanocomposites (136–137 °C) were the same as that of the matrix and are typical of high-density polyethylene (HDPE). However, the crystallization temperatures (T_c) of all nanocomposites were 2–4 °C higher than those of the neat PE, indicating that the filler acts as a nucleating agent.

The thermal stability of neat PE and PE/rGO-CNT-Fe nanocomposites was investigated by thermogravimetric analysis (TGA) (the TGA curves are shown in Supporting Information Figure S6). Table I presents the TGA results of the nanocomposites. It can be seen that with increasing percentage of the filler, the maximum degradation temperatures (T_{max}) of the PE nanocomposites shifts to higher values as compared with the neat PE. It can be seen that in the nanocomposite with 6 wt % of filler, the T_{max} and the onset degradation temperature (T_{onset}) increase by 14 and

Table I. Catalytic Activities and Thermal Properties of PE/rGO-CNT-Fe Nanocomposites

Samples	Filler[a] (%)	Polymer (g)	TGA residue %	Catalytic activity[b]	T_c (°C)	T_m (°C)	X_c (%)	T_{onset} (°C)	T_{max} (°C)
PE	0	5.2	0	693	113	137	59	453	495
PE/GCFe$_1$	1.3	5.6	1.1	514	117	136	58	466	502
PE/GCFe$_2$	2.8	6.6	3.5	232	115	137	58	473	506
PE/GCFe$_3$	6.0	5.6	7.5	108	116	136	55	482	509

[a] Filler = GCFe= RGO + CNT-Fe.
[b] kgPE [Zr]$^{-1}$ h^{-1} bar^{-1}; the amount of Zr calculated by ICP was 0.9411 ± 0.0039 wt % Zr/rGO-CNT-Fe.

29 °C compared with the temperatures of neat PE, showing a significant increase in the thermal stability. This same behavior was already reported for nanocomposites PE/rGO.[25] However, we noticed that in PE/CNT-Fe nanocomposites, there was a decrease in T_{max} down to 4 °C with 2.5 wt % of CNT-Fe in PE, showing that iron acts as a catalyst of degradation.[23] It can be concluded that the thermal stability of PE/rGO-CNT-Fe nanocomposites is mainly transferred by rGO and that the amount of Fe is not enough to influence the degradation of PE. Table I also shows that the percentage of filler calculated from the TGA residue is in close agreement with the percentage of filler calculated from the polymer yield.

The molecular weight of the neat polymer is significantly high (4.4×10^5 g mol^{-1} with a polydispersity of 1.9), which was also confirmed by the high melting temperature of 137 °C. Previous preparations of polyolefin nanocomposites using the same

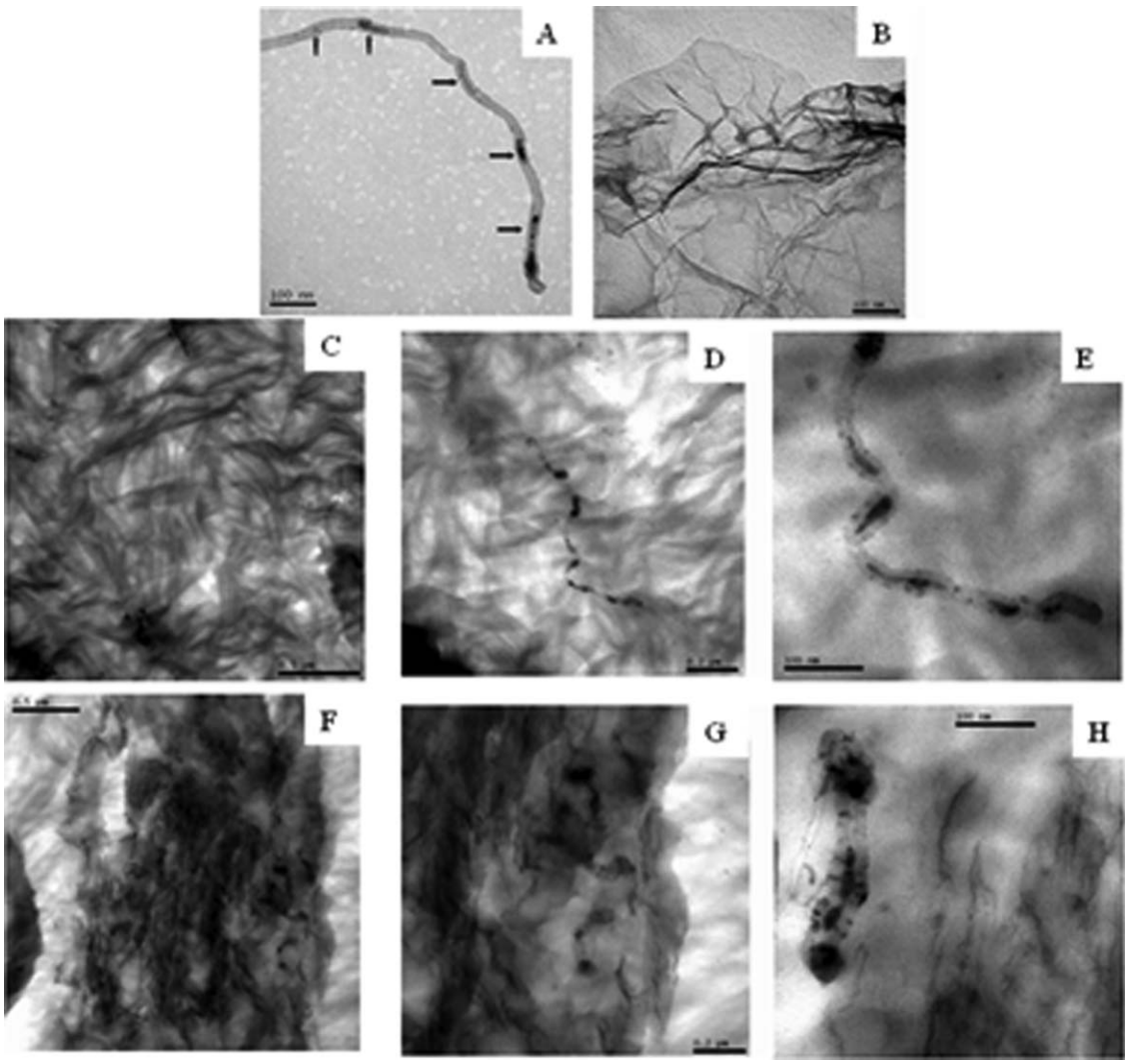

Figure 1. TEM micrographics of CNT-Fe[21] (A), rGO (B), PE/rGO-CNT-Fe nanocomposites 1.3 wt % (C–E), and PE/rGO-CNT-Fe nanocomposites 6.0 wt % (F–H).

Table II. Amount of Iron, CNT-Fe, and rGO in the Nanocomposites

Sample	Filler[a] (%)	CNT-Fe (wt %)	rGO (wt %)	Fe[b] (wt %)	Conductivity (S cm^{-1})	M_R/M_S	H_C (Oe)
PE	0	0	0	0	1.40×10^{-13}	0	0
CNT-Fe	0	100	—	26.9	—	0.32	280
$PE/GCFe_1$	1.3	0.46	0.8	0.04	7.70×10^{-11}	0.51	890
$PE/GCFe_2$	2.8	0.43	2.4	0.04	4.99×10^{-6}	0.52	910
$PE/GCFe_3$	6.0	0.45	5.5	0.06	7.29×10^{-4}	0.52	980

[a] Filler = GCFe = rGO + CNT-Fe.
[b] Fe, from atomic absorption.
Conductivity, normalized remnant magnetization, and coercivity values of nanocomposites of polyethylene with different amounts of reduced graphene oxide and CNT-Fe.

supported method showed that the nanocomposites have higher molecular weight than the neat polymer and maintain the polydispersity close to 2.[14]

The nanocomposites have been studied by TEM to see the morphologies and the dispersion of the fillers. Figure 1 presents the TEM micrographs of CNT-Fe [Figure 1(A)], rGO [Figure 1(B)] and PE/rGO-CNT-Fe nanocomposites with 1.3 wt % [Figure 1(C–E)] and 6.0 wt % [Figure 1(F–H)] of filler at different magnifications. As it can be seen in Figure 1(A), the iron NPs are encapsulated in the CNTs. Figure 1(B) shows the graphene sheets of rGO. All nanocomposites show uniform dispersion of the rGO in the polymer matrix where no aggregation is observed. In Figure 1(D–F,H), isolated CNTs encapsulating iron can be clearly observed. This homogenous dispersion is due to the catalyst supported method where the polymer is formed around the filler during the polymerization reaction. This reveals the advantages of this method over the non-supported catalyst method of polymerization.

The PE/rGO-CNT-Fe nanocomposites were studied by atomic absorption to verify the amount of Fe. Table II reveals that the CNT-Fe contain 26.9 wt % of Fe, and since a fixed amount of CNTs (0.43–0.46 wt %) were added in rGO, the amount of Fe in the nanocomposites remained almost the same, in the range 0.04–0.06 wt %. This is a very low content compared with the total filler (rGO-CNT-Fe) that varied from 1.3 to 6.0 wt %. TEM micrographs also confirm that the amount of Fe is low and that the CNT-Fe is isolated.

One of the most promising aspects of graphene-based materials is their potential for use in various devices and electronics applications, owning to their high electrical conductivity.[37] To obtain conductivity in an insulating matrix, the concentration of the conductive filler must be above the electrical percolation threshold, where a conductive network of filler particles is formed.[38] The percolation threshold is defined as the concentration where a connected assembly of conductive particles is formed in a polymer matrix and lead to a sudden rise in electrical conductivity.[39] One of the objectives of this work is to shift the insulating PE to a semiconductor material to enhance its applications. Table II presents the results of conductivity of the nanocomposites. It can be seen that the electrical conductivity quickly increases from 1.40×10^{-13} S cm^{-1} to 4.99×10^{-6} S cm^{-1} with the addition of only 2.8 wt % of filler, and reaches the highest value of 7.29×10^{-4} S cm^{-1} with 6.0 wt % of the filler. In previous works using *in situ* polymerization, we obtained semi-conductive nanocomposites with conductivities of 1.6×10^{-7} and 1.3×10^{-4} S cm^{-1} at higher amount of graphite nanosheets, 15.3 and 20.9 wt %, respectively.[25] These results are supported by An *et al.*[40] that they reported 10^{-6}–10^{-7} Ω cm for the incorporation of 3.0 wt % of exfoliated graphene (EG) in EG/polypropylene nanocomposites. Recently, Huang *et al.*[41] reported a value of electrical conductivity of 2.3×10^{-5} with the incorporation of 5 wt % of graphene in polypropylene matrix, where we obtained almost this value only with the addition of 2.8 wt % of the filler. The decrease in the percolation threshold can be attributed to two factors, i.e., the excellent exfoliation of rGO used in this work and, most probably, the presence of single graphene sheets that provides better dispersion in the polymer matrix. The second factor is the supporting methodology used for the catalyst that improves the dispersion of the filler and leads to the morphology of graphene sheets.

The room temperature magnetization hysteresis loops of the CNT-Fe powder and PE/rGO-CNT-Fe nanocomposites are plotted in Figure 2 The magnetization data of the PE (not shown) evidence only diamagnetic characteristics. It can be notice that the magnetization of CNT-Fe is almost three times lower than the one of the nanocomposites. The explanation for this behavior is that in the filler the iron NPs are closer than in the nanocomposites where they are well dispersed. Low inter-particle distances enhance demagnetization. The hysteresis loops for the PE/rGO-CNT-Fe samples turned out to be very similar, showing almost an identical value of their remnant magnetization/saturation magnetization ratio (M_R/M_S) of ~0.52, while the coercivity (H_C) varies between 890 and 980 Oe. All H_C and M_R/M_S values of the nanocomposites are given in Table II. The coercivity (H_C) values obtained for the nanocomposites are very high compared with another ferromagnetic nanocomposites in the literature. Composites of poly(aniline-*co*-aminonaphtalenesulfonic acid) with Fe_3O_4 NPs showed coercivity of 15–17 Oe at room temperature.[42] Recently, Sim *et al.*[43] have reported on Fe_3O_4@PANI magnetic materials prepared by oxidation polymerization of PANI on the surface of Fe_3O_4. They have obtained a coercivity of ~40 Oe, which is around 4% of the value in our results. Similarly, Riquelme *et al.*[44] reported coercivity values between 500 and 550 Oe for polypropylene magnetic nanocomposites with 2%–6% of CNT-Fe obtained by melt mixing. Santos *et al.*[45] obtained coercivities of 275 and 250 Oe

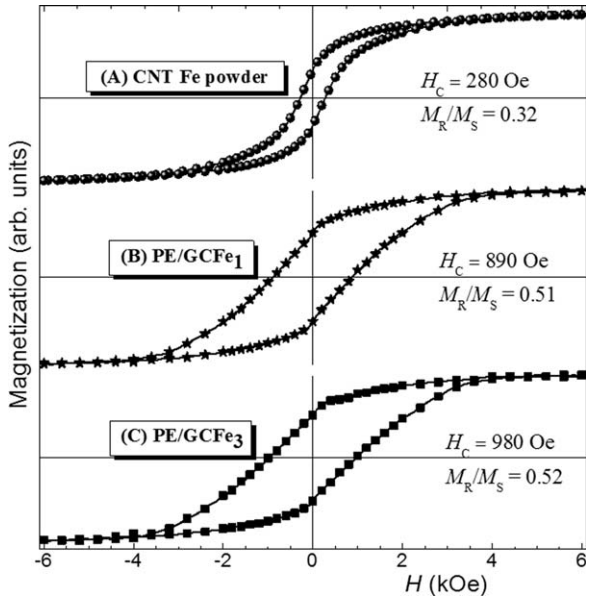

Figure 2. Room temperature hysteresis loops of (A) CNT-Fe powder, (B) PE/GCFe$_1$, and (C) PE/GCFe$_3$ nanocomposites. The lines are only a guide to the eyes.

at 2 K for polyurethanes with 3 and 10 wt % of Fe_3O_4 synthetic talc but any magnetization at room temperature. Reddy *et al.*[46] showed an increase in M_R and M_S from 0.5 to 13.2 and 0.08 to 2.42, respectively, by increasing the amount of Fe_3O_4 from 1 to 30 wt % in poly(3,4 ethylenedioxythiophene), but they reported the absence of hysteresis loop which indicates the superparamagnetic nature of the nanocomposites. He *et al.*[2] reported a decrease in H_C from 193 to 9 Oe with the increase in the amount of magnetic particles from 5 to 20 wt % in a HDPE matrix. This can be attributed to a decrease in the inter-particle distance resulting in stronger, demagnetizing, dipolar interactions; the latter tends to stabilize demagnetized state with low remnant and coercivity values. In our case, the M_R/M_S value of ~0.52 is very close to that (0.5) of systems consisting of non-interacting single-domain particles with uniaxial anisotropy.[47] For such configurations, the H_C value should be approximately twice lower than the anisotropy (or closure) field (H_A), i.e., the magnetic field above which the magnetization processes are only reversible.[48] The fact that in the present case, the values of H_C are rather lower than the respective magnetic anisotropy fields indicates that our samples present a distribution of the strength of their H_A, most probably due to the distribution in the particle sizes. One notes that H_C remains nearly the same, in agreement with the amount of the magnetic constituent (Fe) whose concentration is almost constant (0.04–0.06 wt %). The fact that the mean inter-particle distance remains practically the same in these samples owing to the low amount of magnetic constituent ($\leq$0.06 wt %) indicates an uniform dispersion in the polymer matrix, which is in agreement with TEM data.

CONCLUSIONS

PEs that present both electric and magnetic properties have been obtained. The electric properties have been attained as a result of the rGO turning the PE into a semiconductor. The thermal stability of the nanocomposites was characterized by T_{max} and T_{onset}, which increased by 14 and 29 °C, respectively, with the incorporation of 6 wt % of the filler. The electrical conductivities increased from 4.99×10^{-6} S cm^{-1} with the addition of only 2.8 wt % of the filler and reached 7.29×10^{-4} S cm^{-1} with 6.0 wt % of the filler. Atomic absorption revealed that the amount of Fe was 26.9 wt % in the CNTs and 0.04–0.06 wt % in the nanocomposites; however, the coercivity values were 280 and 890–980 Oe, respectively, confirming that good dispersion and high inter-particle distance can avoid notable dipolar interactions that would tend to stabilize the demagnetized state. The high coercivity values are attributed to the encapsulation of Fe in the CNTs, which protect the magnetic NP from easy oxidation and aggregation in the polymer matrix. These results show that the synthetic CNT-Fe is an interesting material to produce magnetic polymer nanocomposites. TEM also confirmed that there was a good dispersion of CNT-Fe among the rGO and in the PE matrix, revealing isolated CNT-Fe particles.

This material has the potential to be used in a variety of applications, where a flexible magnetic and electrical material with good processability is required, as for example, electromagnetic device application like electromagnetic interference suppression, micro electronics, and aircraft industries.

ACKNOWLEDGMENTS

The authors are grateful to the TWAS-CNPQ for the fellowship to Muhammad Nisar, the CNPq for the special visiting research fellowship to Professor Raúl Quijada, and CNPq grant 302902/2013–9. Professor Raúl Quijada acknowledges the Millennium Nucleus of Chemical Processes and Catalysis (CPC), grant number NC120082. They also thank CME and LRNANO from UFRGS for the microscopy analysis.

REFERENCES

1. Schaefer, D. W.; Justice, R. S. *Macromolecules* **2007**, *40*, 8501.
2. He, Q.; Yuan, T.; Zhu, J.; Luo, Z.; Haldolaarachchige, V.; Sun, L.; Khasanov, A.; Li, Y.; Young, D. P.; Wei, S.; Guo, Z. *Polymer* **2012**, *53*, 3642.
3. Chrissafis, K.; Paraskevopoulos, K. M.; Tsiaoussis, I.; Bikiaris, D. C. *J. Appl. Polym. Sci.* **2009**, *114*, 1606.
4. Coleman, J. N.; Khan, U.; Blau, W. J.; Gun'ko, Y. K. *Carbon* **2006**, *44*, 1624.
5. Reddy, K. R.; Sin, B. C.; Yoo, C. H.; Sohn, D.; Lee, Y. *J. Colloid Interface Sci.* **2009**, *340*, 160.
6. Kuila, T.; Bose, S.; Mishra, A. K.; Khanra, P.; Kim, N. H.; Lee, J. H. *Polym. Test.* **2012**, *31*, 31.
7. Andrews, R.; Weisenberger, M. C. *Curr. Opin. Solid Stat. Mater.* **2004**, *8*, 31.
8. Ma, P. C.; Siddiqui, N. A.; Marom, G.; Kim, J. K. *Compos. Part A: Appl. Sci. Manuf.* **2010**, *41*, 1345.
9. Raghu, A. V.; Jeong, H. M.; Lee, Y.; Raghu, A. V. *J. Polym. Sci. Part A: Polym. Chem.* **2010**, *48*, 1477.

10. Kim, H.; Abdala, A. A.; Macosko, C. W. *Macromolecules* **2010**, *43*, 6515.
11. Geim, A. K.; Novoselov, K. S. *Nat. Mater.* **2007**, *6*, 183.
12. Dikin, D. A.; Stankovich, S.; Zimney, E. J.; Piner, R. D.; Dommett, G. H. B.; Evmenenko, G.; Nguyen, S. T.; Ruoff, R. S. *Nature* **2007**, *488*, 457.
13. Wakabayashi, K.; Pierre, C.; Dikin, D. A.; Rouff, R. S.; Ramanathan, T.; Brinson, L. C.; Torkelson, J. M. *Macromolecules* **2008**, *41*, 1905.
14. Pavoski, G.; Maraschin, T.; Milani, M. A.; Azambuja, D. S.; Quijada, R.; Moura, C. M.; Basso, N. R. S.; Galland, G. B. *Polymer* **2015**, *81*, 79.
15. Hassan, M.; Reddy, R. K.; Hague, E.; Minett, A. I.; Gomes, V. G. *J. Colloid Interface Sci.* **2013**, *410*, 43.
16. Han, S. J.; Lee, H.; Jeong, H. M.; Kim, B. K.; Raghu, A. V.; Reddy, K. R. *J. Macromol. Sci. Part B: Phys.* **2014**, *53*, 1193.
17. Son, D. R.; Raghu, A. V.; Reddy, K. R.; Jeong, H. M. *J. Macromol. Sci. Part B: Phys.* **2016**, *55*, 1099.
18. Hassan, M.; Reddy, K. R.; Hague, E.; Faisal, S. N.; Ghasemi, S. *Compos. Sci. Technol.* **2014**, *98*, 1.
19. Lee, Y. R.; Kim, S. C.; Lee, H.; Jeong, H. M.; Raghu, A. V.; Reddy, R. K.; Kim, B. K. *Macromol. Res.* **2011**, *19*, 66.
20. Schinteie, G.; Kuncser, V.; Palade, P.; Alexandrescu, R.; Morjan, I.; Filoti, G. *J. Alloy Compd.* **2013**, *564*, 27.
21. Osorio, A. G.; Bergmann, C. P. *Appl. Surf. Sci.* **2013**, *264*, 794.
22. Osorio, A. G.; Pereira, L. G.; Cunha da, J. B. M.; Bergmann, C. P. *Mater. Res. Bull.* **2013**, *48*, 4168.
23. Nisar, M.; Bergmann, C.; Geshev, J.; Quijada, R.; Galland, G. B. *Polymer* **2016**, *97*, 131.
24. Milani, M. A.; González, D.; Quijada, R.; Basso, N. R. S.; Cerrada, M. L.; Azambuja, D. S.; Galland, G. B. *Compos. Sci. Technol.* **2013**, *84*, 1.
25. Fim, F. C.; Basso, N. R. S.; Graebin, D. S.; Azambuja, D. S.; Galland, G. B. *J. Appl. Polym. Sci.* **2013**, *128*, 2630.
26. Milani, M. A.; González, D.; Quijada, R.; Benavente, R.; Arranz-Andrés, J.; Galland, G. B. *Polymer* **2015**, *65*, 134.
27. Fim, F. C.; Guterres, J. M.; Basso, N. R. S.; Galland, G. B. *J. Polym. Sci. Part A: Polym. Chem.* **2010**, *48*, 692.
28. Kim, P.; Doss, N. M.; Tillotson, J. P.; Hotchkiss, P. J.; Pan, M. J.; Marder, S. R.; Li, J.; Calame, J. P.; Perry, J. W. *ACS Nano* **2009**, *3*, 2581.
29. Dai, Q.; Berman, D.; Virwani, K.; Frommer, J.; Jubert, P. O.; Lam, M.; Topuria, T.; Imaino, W.; Nelso, A. *Nano Lett.* **2010**, *10*, 3216.
30. Shimad, T.; Ookubo, K.; Komuro, N.; Shimizu, T.; Uehara, N. *Langmuir* **2007**, *23*, 11225.
31. Guo, Z.; lee, S. E.; Kim, H.; Park, S.; Hahn, H. T.; Karki, A. B.; Young, D. P. *Acta Mater.* **2009**, *57*, 267.
32. Staudenmaier, L. *Chem. Ges.* **1898**, *31*, 1481.
33. Pavoski, G.; Maraschin, T.; Fim, F. C.; Balzaretti, N. M.; Galland, G. B.; Moura, C. S.; Basso, N. R. S. *Mater. Res.* **2017**, *20*, 53.
34. Resano, M.; Bolea-Fernández, E.; Mozas, E.; Flórez, M. R.; Gringberg, P.; Sturgeon, R. E. *J. Anal. At. Spectrom.* **2013**, *28*, 657.
35. Stürzel, M.; Kempe, F.; Thomann, Y.; Mark, S.; Enders, M.; Mülhaupt, R. *Macromolecules* **2012**, *45*, 6878.
36. Tait, P. J.; Ediati, R. In Metalorganic Catalysts for Synthesis and Polymerization; Kaminsky, W., Ed.; Springer. Heidelberg, **1999**; p 307.
37. Potts, J. R.; Dreyer, D. R.; Bielawski, C. W.; Ruoff, R. S. *Polymer* **2011**, *52*, 5.
38. Balogum, Y. A.; Buchanan, R. C. *Compos. Sci. Technol.* **2010**, 885.
39. Kuilla, T.; Bhadrab, S.; Yao, D.; Kim, N. H.; Bose, S.; Lee, J. H. *Prog. Polym. Sci.* **2010**, *35*, 1350.
40. An, J. E.; jeon, G. W.; jeong, Y. G. *Fiber Polym.* **2012**, *13*, 507.
41. Huang, C. L.; Lou, C. W.; Liu, C. F.; Huang, C. H.; Song, X. M. *Appl. Sci.* **2015**, *5*, 1196.
42. Reddy, K. R.; Lee, K. P.; Gopalan, A. I. *J. Appl. Polym. Sci.* **2007**, *106*, 1181.
43. Sim, B.; Chae, H. S.; Choi, H. J. *eXPRESS Polym. Lett.* **2015**, *9*, 736.
44. Riquelme, J.; Garzón, C. A.; Bergmann, C. P.; Geshev, J.; Quijada, R. *Eur. Polym. J.* **2016**, *75*, 200.
45. Santos, L. M. D.; Ligabue, R.; Dumas, A.; Roux, C. L.; Micoud, P.; Meunier, J. F.; Martin, F.; Einloft, S. *Eur. Polym. J.* **2015**, *69*, 38.
46. Reddy, K. R.; Park, W.; Sin, B. C.; Noh, J.; Lee, Y. *J. Colloid Interface Sci.* **2009**, *335*, 34.
47. Stoner, E. C.; Wohlfarth, E. P. *Philos. Trans. R. Soc. Lond. Ser. A* **1948**, *240*, 559.
48. Harres, A.; Mikhov, M.; Skumryev, V.; de Andrade, A. M. H.; Schmidt, J. E.; Geshev, J. *J. Magn. Magn. Mater.* **2016**, *402*, 76.